Key Engineering Materials
ISSN: 1662-9795, Vol. 926, pp 547-558
doi:10.4028/p-51lv37

Submitted: 2021-12-01
Revised: 2022-01-25
Accepted: 2022-01-25
Online: 2022-07-22

Methodology to Investigate the Transformation Plasticity for Numerical Modelling of Hot Forging Processes

Bernd-Arno Behrens[1,a], Kai Brunotte[1,b], Hendrik Wester[1,c] and Christoph Kock[1,d*]

[1]Institut für Umformtechnik und Umformmaschinen (IFUM), Leibniz Universität Hannover (LUH), An der Universität 2, Garbsen 30823, Germany

[a]behrens@ifum.uni-hannover.de, [b]brunotte@ifum.uni-hannover.de, [c]wester@ifum.uni-hannover.de, [d]kock@ifum.uni-hannover.de

*corresponding author

Keywords: Hot forging, FE-simulation, phase transformation, transformation-induced plasticity, Gleeble 3800-GTC, AISI 4140, AISI 52100

Abstract. Hot forging is a complex process involving the mutual influence of numerous thermo-mechanical-metallurgical material phenomena. In particular, the strains of transformation-induced plasticity (TRIP) have a significant influence on the distortions and residual stresses of the components. The TRIP strains refer to the anisotropic strains depending on the orientation and significance of the stress conditions during cooling superimposed to the phase transformation. With the use of numerical models, the impact of this effect can be investigated in order to ensure the production of high quality components. However, an experimental determination of the characteristic values of TRIP is challenging, which is why only few corresponding data are available in the literature. Therefore, this paper presents an experimental and numerical methodology as well as the results of studies on the interaction between stresses and phase transformations in the materials AISI 4140 and AISI 52100. The investigations of the TRIP strains are carried out using hollow specimens, which are thermo-mechanically treated in the physical forming simulator Gleeble 3800-GTC. The specimens are austenitised, quenched to test temperature and held there while diffusion controlled phase transformation takes place. The extent of TRIP as a result of different superimposed tensile or compressive loads is determined by means of dilatometry. In addition, the extent of TRIP for diffusionless martensitic phase transformations was investigated by continuous cooling tests under tensile and compressive loads. It was found that the transformation plasticity varies depending on the material, the phase type, the temperature and the tensile or compressive stresses. Subsequently, simulations of the physical experiments using the FE software Simufact. Forming verified the determined phase specific values of TRIP.

Introduction

Forging processes have proven valuable in industrial mechanical engineering for the production of complex and heavily loaded components [1]. The high forming temperatures of up to 1250 °C reduce the yield stress, which enables improved material flow, decreased forming forces and thus the production of geometrically challenging parts. At the same time, the forging process generates a fine microstructure in the material, which results in advantageous strength and service life properties [2]. However, designing a hot forming process is challenging as numerous influencing parameters interact with each other, which makes a purely analytical consideration impossible [3]. As shown in Fig. 1a, there are close relationships between mechanical, thermal and metallurgical material phenomena, defining the final properties of the component according to the chemical composition of the material. For this reason, hot forming processes are often designed using the finite element (FE) method. Due to the numerous influencing parameters in the thermo-mechanical-metallurgical process, this represents a challenge. In order to compute these processes, the additive strain decomposition method was used for instance by *Denis et al.* [4] for calculation of stresses during quenching of a cylindrical specimen from a low alloy steel or by *Behrens et al.* [5] in order to simulation press hardening of a

manganese-boron steel. Thereby, the five parameters of elastic, plastic, thermal, transformation related and transformation plasticity strains are considered separately and summed up to the total strain increment as shown in Fig. 1b.

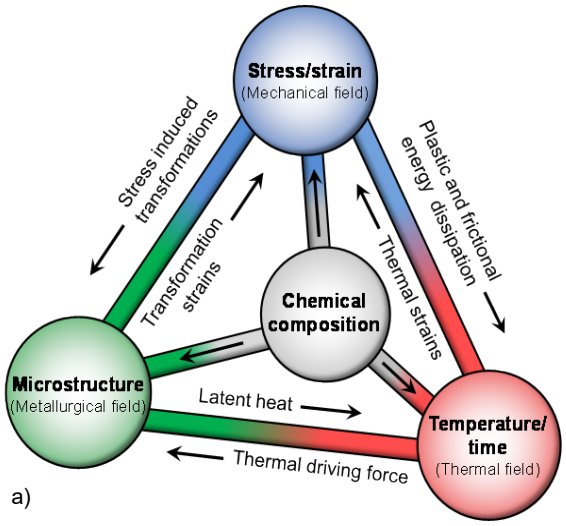

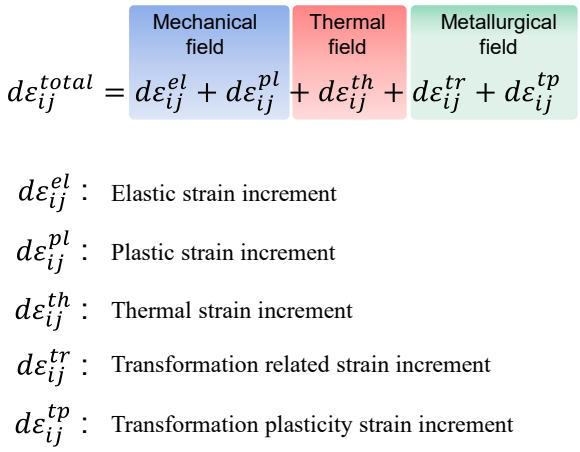

Fig. 1: Interrelated thermo-mechanical-metallurgical material phenomena during thermo-mechanical processing of steel (a) and basic principles of the additive strain decomposition method (b) according to [6].

The transformation related strains denote the volumetric strains experienced by a polymorphic material as a result of the phase transformations. Thereby, austenite with a face-centered cubic lattice transforms to the microstructural constituents ferrite, pearlite, bainite or martensite with a body-centered cubic lattice or body-centered tetragonal lattice. In a stress-free state, these strains are of isotropic nature. However, if the phase transformation is superimposed by a stress, anisotropic transformation strains occur. For instance, in the case of uniaxial tensile stress, the strain is increased in the direction of the predominant stress, while smaller strains result in the other directions in accordance with the volume constancy. This effect is described by the transformation plasticity strains.

From the perspective of material characterisation, the acquisition of characteristic values of elastic, plastic and thermal strain behaviour is already well researched and numerous literature data are available concerning these aspects [7]. To model the elastic strains, Young's moduli are usually determined in tensile tests[8]. The plastic deformation behaviour can be described based on flow curves from uniaxial upsetting tests [9]. Likewise, the coefficients of thermal expansion to simulate thermal expansion can be determined in dilatometric studies, e. g. according to [10].

In contrast, there are far fewer norms and standards for the characterisation of material phenomena resulting from metallurgical effects and the acquisition of such material data requires special equipment. Therefore, material data can hardly be found in the literature in this regard. At present, guidelines only exist for determining the transformation times in the form of continuous cooling transformation (cct) or time temperature transformation (ttt) diagrams, such as the ASTM A1033 [11]. From an engineering point of view, these cct and ttt diagrams provide a reasonable guide for the design of heat treatment programs. However, these can only be used to draw conclusions about the transformation times and the amount of the transformed phase fraction. The previously mentioned transformation related and transformation plasticity strains cannot be calculated based on this data. Particularly these data are crucial to optimise forging processes regarding the development of distortion and residual stresses [12]. For the calculation of transformation related strains, the approach shown in equation (1) is often reported in the literature [13].

$$d\varepsilon_{ij}^{tr} = \sum_{ph}\left(\frac{\Delta V_{tr}}{V_0}\right)_{A\rightarrow ph} d\xi_{ph}\delta_{ij} \tag{1}$$

In this context, $(\Delta V_{tr}/V_0)_{A\rightarrow ph}$ denotes the volumetric strain that occurs when the austenite is completely transformed into phase *ph*, $d\xi$ is the incremental proportion of the transformed phase *ph* and δ_{ij} represents the Kronecker delta, which is used to account for the strains in the main directions of strain. The growth of the phase can be determined from ttt diagrams, as described in [14]. The phase-specific volume expansion, on the other hand, cannot be determined from ttt diagrams. *Simsir* [13] calculates this constant via the density-ratio of the parent and the emerging phase for simulation of residual stress development in different carbon steels due to a heat treatment. *Olle* [15] utilised the ratios of the lattice constants at each phase from literature data [16] to calculate $(\Delta V_{tr}/V_0)_{A\rightarrow ph}$ for press hardening simulation of a manganese-boron steel. Friction welding of a carbon steel and a low alloy steel was simulated by *Chugreev* [17] using data for $(\Delta V_{tr}/V_0)_{A\rightarrow ph}$ from the thermo-dynamic material simulation software JMatPro [18, 19]. As these three examples of application show, for the process simulation, theoretical values were used with regard to $(\Delta V_{tr})_{A\rightarrow ph}$. In the field of experimental material characterisation, the diffusion-controlled phase transformations of an AISI 52100 were investigated by *Dalgic et al.* [20] with regard to its volume expansions. The volume change of partially hollow specimens after austenitisation at 850 °C was investigated at different isothermal test temperatures by means of two dilatometers in a Gleeble system. In addition, the $(\Delta V_{tr}/V_0)_{A\rightarrow ph}$ for a low-alloy and a carburised steel were also investigated by *Ahrens* [21] on hollow specimens after austenitisation at 860 °C using two dilatometers in a universal testing machine. Few volume change data can be found in the literature for other forging steels and the corresponding austenitisation temperature of more than 900 °C relevant for hot forming.

To account for the anisotropy of the transformation strains under a superimposed stress, equation (2) can be used, where K_{ph}^{tp} is the phase-specific coefficient of the transformation plasticity. In addition to K_{ph}^{tp}, the stress deviator S_{ij} and a function of the current fraction of the emerging phase describing the evolution of transformation plasticity are included in the calculation. As shown in equation (3) K_{ph}^{tp} is a proportionality factor between transformation plasticity strain and the superimposed stress [22]. For the function of transformation evolution $f(\xi)$, there are several approaches from authors like *Abrassart* [23], *Sjöström* [24] and *Fischer et al.* [25] which are used depending on the material type. However, the approach by *Leblond* [26] in equation (4) is most commonly used.

$$d\varepsilon_{ij}^{tp} = K_{ph}^{tp} S_{ij} f(\xi_{ph}) \tag{2}$$

$$K_{ph}^{tp} \propto \frac{d\varepsilon_{ij}^{tp}}{S_{ij}} \tag{3}$$

$$d\varepsilon_{ij}^{tp} = \frac{3}{2} K_{ph}^{tp} \frac{df(\xi_{ph})}{d\xi_{ph}} d\xi_{ph} S_{ij} \qquad \text{where } f(\xi_{ph}) = \xi_{ph}(1 - \ln(\xi_{ph})) \tag{4}$$

There are different approaches in the literature for determining K_{ph}^{tp}. The aforementioned authors calculate K_{ph}^{tp} from the yield strength of the austenitic phase as well as the constant $(\Delta V_{tr}/V_0)_{A\rightarrow ph}$ and further material dependent coefficients [27]. This type of approach is used, for example, from *Behrens et al. [14]* to simulate a press hardening process of a manganese-boron steel. A similar process is simulated by *Olle* [15] using literature data for the manganese-boron steel from [28] for the bainitic and martensitic phase transformation. Thereby, a differentiation is made between the stress types tension ($K_{ph}^{tp} = 8.68 * 10^{-5}$ MPa^{-1}) and compression ($K_{ph}^{tp} = 9.33 * 10^{-5}$ MPa^{-1}). For the simulation of friction welding processes, phase-specific and temperature-dependent coefficients K_{ph}^{tp} for a carbon steel and a low alloy steel are calculated by *Chugreev* [17] using JMatPro. This shows that process simulations are mostly relying on highly simplified models based on theoretical material data or on generalised experimental data. However, some experimental work show that the transformation temperature, the type of transformation and the applied stress state (tension/compression) significantly influence transformation plasticity. For example, *Ahrens* [21] investigated the transformation plasticity of a low-alloy steel and a carburised low-alloy steel after austenitisation at 860 °C. Thereby, constants from $K_{ph}^{tp} = 4$ to $9 * 10^{-5}$ MPa^{-1} were found, depending on the phasetype and temperature as well as on the type of stress. Furthermore, it was found that a superimposed stress

increases the phase transformation rate. *Besserdich et al.* [29] studied the martensitic phase transformation of AISI 4140 after austenitisation at 860 °C, where $K_{ph}^{tp} = 4.2 * 10^{-5}$ MPa^{-1} was determined. *Behrens et al.* [30] also investigated the martensitic phase transformation of the alloy AISI 4140 and found similar results as *Besserdich*. Besides, it has been discovered that the austenitisation temperature (950 °C compared with 1200 °C) has an influence on the extent of transformation plasticity and thus on K_{ph}^{tp}. Furthermore, *Dalgic et al.* [20] studied transformation plasticity with superimposed tensile loads during diffusion controlled phase transformation of AISI 52100 after austenitisation at 850 °C for temperatures in the range of 300 °C to 700 °C. They determined constants of about $K_{ph}^{tp} = 6$ to $15 * 10^{-5}$, varying the transformation temperature and the type of transformation.

From this literature review, it can be deduced that, on the one hand, the consideration of phase transformations in hot forming process simulations is crucial for the calculation of distortion and residual stresses as it is taken into account in many applications. On the other hand, theoretical or generalised material parameters are often used for the phase transformation simulations, which leads to imprecise results. This is due to the fact that up to now only few experimental data are available for the corresponding conditions, such as austenitisation temperatures typical for hot forming, phase-specific and temperature-dependent data as well as data for superimposed tensile and compressive stresses. In turn, this can be explained by the complex and so far non-standardised determination procedures that require special technical equipment. As some fundamental research work has shown, there is a significant relation between K_{ph}^{tp} and the aforementioned conditions. Therefore, the aim of this work is to present a method for determining the constant K_{ph}^{tp} depending on these conditions in the Gleeble system. In addition, this work is intended to create a database for the two typical forging steels investigated, AISI 4140 and AISI 52100, for use in hot forming simulations.

Methodology for the Investigation of Transformation-Induced Plasticity

Investigated Materials. For the investigations in this work, two different typical hot-forging steel alloys were used. The first one was alloy AISI 52100, also referred to as 1.3505 according to the international standard ISO 683-17 [31], which is typically used for the production of roller bearing rings. The second one was alloy AISI 4140, also referred to as 1.7225 according to the international standard ISO 683-1 [32], which is used as heat-treatable steel for highly-loaded components, for example in the automotive sector. The chemical compositions provided by the supplier are listed in Table 1.

Table 1: Chemical composition of steel alloys AISI 52100 and AISI 4140.

[wt%]	*C*	*Si*	*Mn*	*P*	*S*	*Cr*	*Mo*	*Fe*
AISI 52100	0.99	0.20	0.35	0.011	0.014	1.44	0.01	Balance
AISI 4140	0.42	0.19	0.82	0.009	0.024	1.04	0.16	Balance

Experimental set-up at the Gleeble 3800-GTC. The principle test setup used at the Gleeble 3800-GTC is presented in Fig. 2a. The Gleeble is prepared with the so-called low-force testing apparatus, which allows high-precision force measurement via a load cell of up to 20 kN. Fig. 2b shows an installed specimen with the attached lengthwise extensometer, while the geometry of the used hollow specimen is shown in Fig. 2c. To realise high cooling rates from the austenitisation temperature to the test temperature, this thin-walled specimen can be cooled with nitrogen from the inside via the bore. During the tests, the strain of the specimens was measured by two extensometers, a lengthwise and a crosswise extensometer, respectively, as shown in Fig. 2d. The specimen is clamped in the custom-made grips by means of M12 threads. Clamping via threads allows both tensile and compressive loads to be applied to the specimen. One side has a left-hand thread, the other a right-hand thread. This ensures that the specimen does not move as a result of thermal expansion during heating. The lengthwise extensometer is a full-bridged strain gauged design transducer of the type HZT071 from DSI Inc. with a resolution of ±2 µm. The push rods are pressed onto the specimen via ceramic fiber cords. The crosswise extensometer is a linear variable differential transducer based

dilatometer type 39018 from DSI Inc. with a resolution of ±0.4 µm. The specimen is placed between the angled push rods, which are preloaded with a low spring force. Both of the gauges can be used permanently at specimen temperatures in the range of 10 °C and 1200 °C.

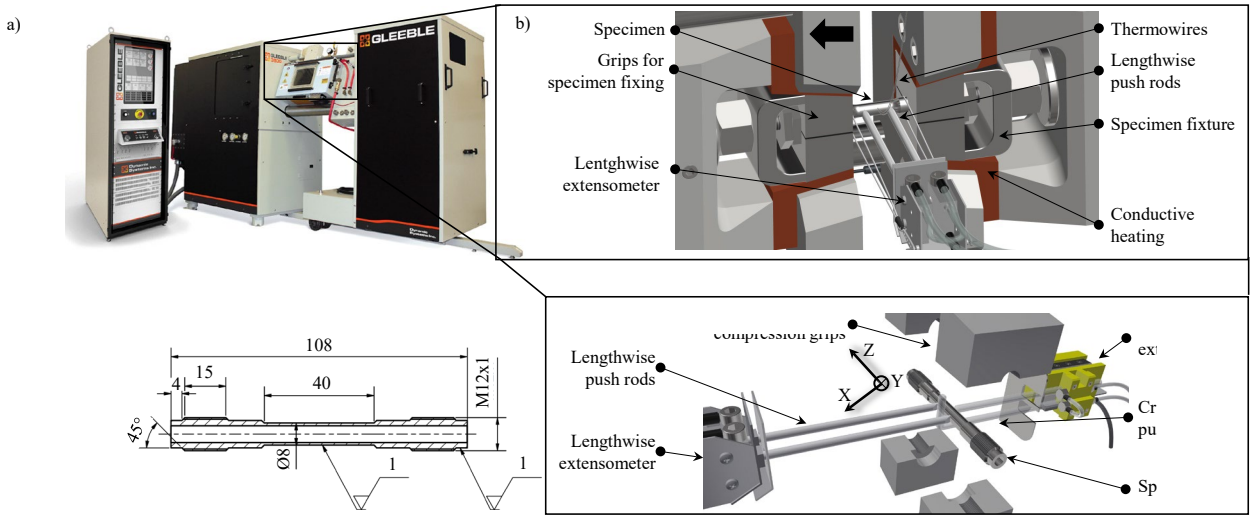

Fig. 2: Gleeble 3800-GTC (a) with an illustration of the general setup for tensile-compression experiments (b), specimen geometry (c) as well as specified setup (d) for the investigation of the metallurgical material data.

Numerical model for verification of acquired material data. For the verification and further calibration of the experimentally determined material data, a simulation model of the tests was developed in the heat treatment module of the commercial software Simufact.Forming 16. Calculation was carried out based on MSC.Marc-Solver. The experimental temperature profiles shown in Fig. 4b are applied as boundary conditions in order to simulate the transformation related- and transformation plasticity effects. The principle design is shown in Fig. 3a. Within in the model only the relevant centre section of the specimen with the measuring length of 18 mm was considered and modelled using rotational symmetry by 332 quad-elements of MSC.Marc-Type 10. In order to model the tensile or compressive forces, the auxiliary modelling tools A and B are used, which feature no heat transfer to the specimen. The auxiliary modelling tools are bonded to the specimen, whereby the movements of the specimen in x- and y-direction are permitted without friction. The tensile or compressive forces are generated in Simufact.Forming via generic spring A and B, on which table driven force profiles can be applied. Since the applied superimposed forces in this study do not cause plastic deformations at any test temperature, but are in the elastic range, it is sufficient to use only elastic material parameters in the simulations. Therefore, the elastic Young's moduli were calculated by JMatPro based on the chemical composition of the alloys (Table 1) and are listed in Table 2. For both materials the Poisson's ratio $\nu = 0.3$ was used.

Table 2: Young's moduli of AISI 52100 and AISI 4140 calculated by JMatPro.

	Young's moduli [MPa]				
Temperature [°C]	***25***	***400***	***500***	***600***	***700***
AISI 52100	210111	184354	173445	161111	147623
AISI 4140	21106	184466	172949	159867	145563

The coefficients of thermal expansion for the austenitic phase were determined from the experimental results described in the next section according to equation (5). To calculate the coefficient of thermal expansion from austenite, the quotient of the strain difference and temperature difference obtained during cooling from 1000 °C to the martensite start temperature in the diffusionless phase transformation experiments was determined. For AISI 4140 $\alpha_A = 2.43906 * 10^{-5}$ K^{-1} and for AISI 52100 $\alpha_A = 2.63616 * 10^{-5}$ K^{-1} were identified. To calculate the coefficient of thermal expansion of martensite, after completed cooling to room temperature, the specimens were

reheated to martensitestart temperature and the quotient from the strain difference and temperature difference between martensite start temperature and room temperature was determined. For AISI 52100 $\alpha_M = 1.18155 * 10^{-5}$ K^{-1} and for AISI 4140 $\alpha_M = 1.29589 * 10^{-5}$ K^{-1} were identified. To model the phase transformation onset and duration, ttt diagrams were taken from a previous work of the authors concerning the investigated materials [33].

$$\alpha_p = \frac{\Delta\varepsilon_l}{\Delta T} \tag{5}$$

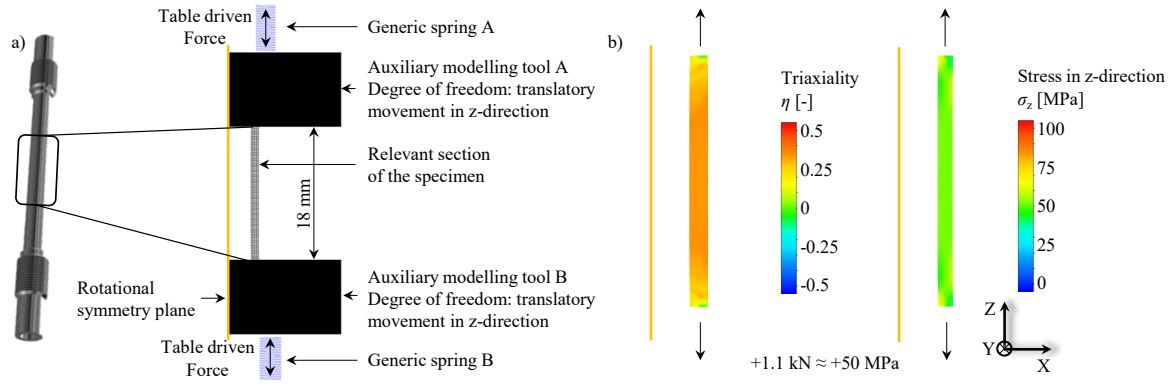

Fig. 3: Schematic design of the simulation model for the characterisation tests (a) and demonstration of the approximately uniform uniaxial stress state and the stress distribution in the z-direction from an exemplary test with AISI 52100 at 600 °C and a superimposed load of 1.1 kN (b).

Procedure for determining the metallurgical material data. For investigation of metallurgical material data, the specimens are heated with a heating rate of 10 K/s to the austenitisation temperature of 1000 °C and held there for 300 s. Subsequently, to investigate the diffusion-controlled phase transformations, the specimens are quenched at a cooling rate of 60 K/s in average to the respective test temperature T_{tr} and held at this temperature until the phase transformation is complete. In the case of investigating diffusionless phase transformations, the specimens were cooled down to room temperature at a constant rate of $\dot{T}_{cr} = 10$ K/s. Immediately before the start of the phase transformation, the force to be investigated was applied to the specimen within 3 s in each case. As the experimental plan in Fig. 4b shows, axial stresses $\sigma_L = 0$, ±12.5, ±25 or ±50 MPa were applied depending on the test temperature. According to the dimensions of the specimen in Fig. 2c, this corresponds to forces of about 0, 0.27, 0.55 or 1.1 kN.

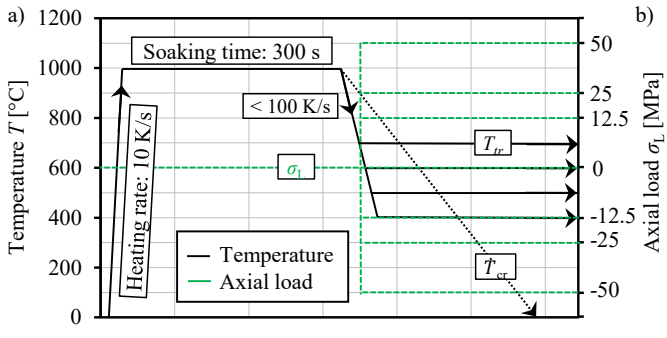

Experimental plan for AISI 4140 and AISI 52100	
Diffusion controlled phase transformations	
Transformation temperature T_{tr}	Superimposed load σ_L
700 °C	0; ±12.5; ±25
600 °C	0; ±25; ±50
500 °C	0; ±25; ±50
400 °C	0; ±25; ±50
Diffusionless phase transformations	
Transformation cooling rate $\dot{T}_{cr}$	Superimposed load σ_L
10 K/s	0; ±25; ±50

Fig. 4: Procedure of the test with regard to temperature and superimposed force (a) as well as experimental plan for the materials AISI 4140 and 52100 (b).

Before the investigation of the transformation plasticity can be conducted, the transformation related volumetric strains $(\Delta V_{tr}/V_0)_{A\rightarrow ph}$ in the stress-free state must be determined. As explained in the introduction, the transformation plastic strains solely describe the anisotropic deviations occurring under certain stresses from the purely isotropic transformation related strains. For the simulation of the transformation plasticity strains, the transformation related strains must therefore be calculated first. From the measurement data of the length change Δl(t) as well as the diameter change Δd(t), the

strains in length direction $\varepsilon_l(t)$ as well as in crosswise direction $\varepsilon_d(t)$ can be computed using equation (6). Subsequently, the volume change $\Delta V/V_0(t)$ as a function of time can be calculated, considering small displacements [21]. The experiments were evaluated with the constants l_0, d_0 and V_0 set to the values present at the time t_0 at the beginning of phase transformation for initial length, diameter as well as volume. Accordingly, the volumetric strains $(\Delta V_{tr}/V_0)_{A\rightarrow ph}$ equals the volume change at the time t_1 at finishing of phase transformation. The times for the beginning and end of the respective phase transformations were determined graphically by applying tangents to the ε_l-t-courses [34]. In addition, the volume expansion can be used to calculate the proportion of the emerging phase $\xi_{ph}(t)$ as a function of time according to equation (7). In this way, it can be subsequently investigated to what extent the transformation rate is influenced by the superimposed force.

$$\frac{\Delta V}{V_0}(t) = \big(1+\varepsilon_l(t)\big)\big(1+\varepsilon_d(t)\big)^2 - 1 \qquad \text{where } \varepsilon_l(t) = \frac{\Delta l(t)}{l_0};\ \varepsilon_d(t) = \frac{\Delta d(t)}{d_0} \tag{6}$$

$$\xi_{ph}(t) = \frac{\frac{\Delta V}{V_0}(t)}{\frac{\Delta V}{V_0}(t_0)} \tag{7}$$

Following the stress-free experiments, the tests were simulated for further calibration of the values $(\Delta V_{tr}/V_0)_{A\rightarrow ph}$ and the ttt diagrams used. Subsequently, the experimental investigations are carried out with superimposed force according to the experimental plan in Fig. 4b. The transformation plasticity strains are calculated at the end of the phase transformation according to equation (8).

$$\varepsilon_{tp,l} = \varepsilon_l(t_1, \sigma_L) - \varepsilon_l(t_1, \sigma_L = 0) \tag{8}$$

Results from the Investigations of Transformation-Induced Plasticity

Material data characterising the transformation related volumetric strains. The data from ttt diagrams describing the transformation times as well as the transformation-related volumetric strains $(\Delta V_{tr}/V_0)_{A\rightarrow ph}$ represent the basis of the investigations on transformation plasticity. For the simulation of the experimental tests, the ttt diagrams from a previous work of the authors [33] were used and further calibrated on the basis of the stress-free tests. As the results in Fig. 5 show, the two materials have a differing transformation behaviour. Common to both materials is the transformation of the ferritic/perlitic phase at 700 °C and 600 °C as well as the bainitic transformation at 500 °C and 400 °C. It can be concluded, that a pure transformation of the respective phase takes place at these testing temperatures, which is why they were chosen in Fig. 4b for investigating the phase-specific and temperature-dependent transformation plasticity characteristics.

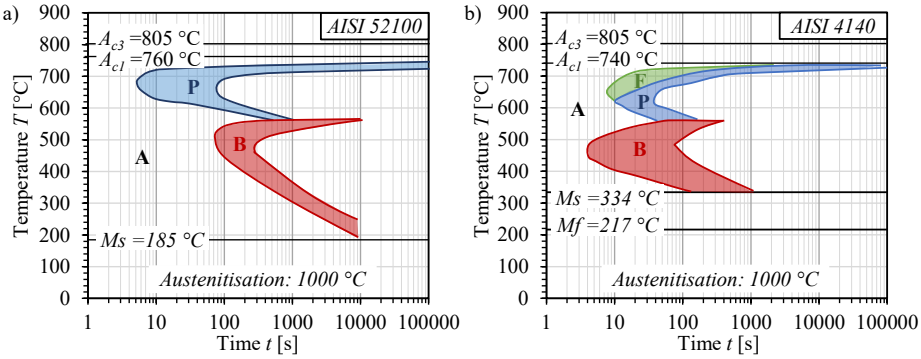

Fig. 5: Calibrated ttt diagrams using stress-free experiments based on the results for AISI 52100 (a) and 4140 (b).

According to equations (6) and (7), the volumetric strains $(\Delta V_{tr}/V_0)_{A\rightarrow ph}$ for the two materials at different temperatures and the different phases were calculated using the stress-free test results. The results are presented in context with the data from the JMatPro calculation software in Fig. 6 for evaluation purposes. It should be noted that two different temperatures were considered for the ferritic/perlitic and the bainitic phase transformation. However, since the martensitic phase transformation cannot

take place under isothermal conditions, only one $(\Delta V_{tr}/V_0)_{A\rightarrow ph}$ was calculated for each of these at the continuous cooling rate of 10 K/s. For both materials, there is a clear temperature and phase dependence. The data calculated by JMatPro for the material charges from Table 1 tend to underestimate the experimental results.

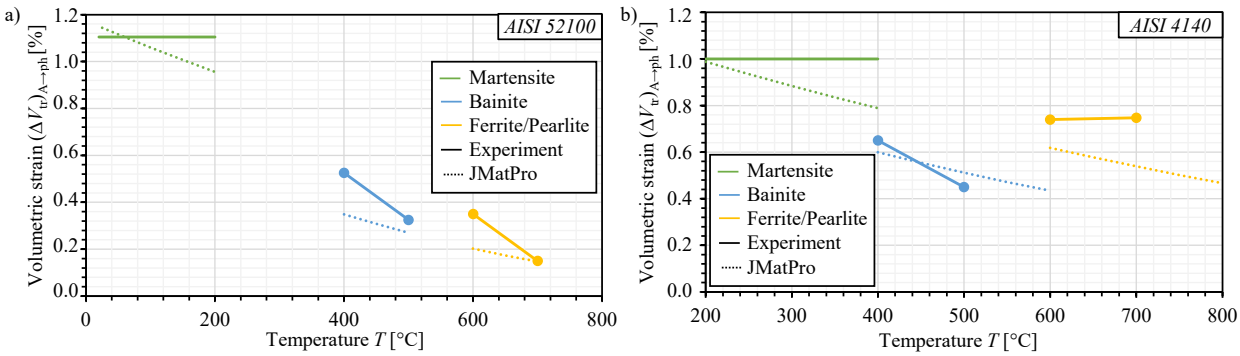

Fig. 6: Results of volumetric strains from stress free experiments in comparison with values from JMatPro for AISI 52100 (a) and 4140 (b).

Material data characterising the anisotropic strains due to transformation plasticity. After the data for the ttt diagrams and the volumetric strains $(\Delta V_{tr}/V_0)_{A\rightarrow ph}$ were adjusted by numerical simulations, the experimental tests with superimposed loads were carried out according to the experimental plan in Fig. 4b. The experimental results are exemplarily shown in Fig. 7a and b for AISI 52100 and isothermal transformation at 600 °C, whereby $\varepsilon_{tp,l}$ and $\varepsilon_{tp,d}$ were calculated by means of equations (6). Using the transformation plasticity lengthwise strains $\varepsilon_{tp,l}$, the K_{ph}^{tp} was determined via equation (3) and further calibrated by a comparison with the simulation results. As a result, the investigated materials showed a clear transformation plasticity effect at all temperatures and for all phase types. For the isothermal pearlitic transformation at 600 °C of AISI 52100, for example, a transformation plasticity lengthwise strain of $\varepsilon_{tp,l} = 0.6$ % was determined at a tensile stress of $\sigma_L = 50$ MPa. In contrast, at the compressive stress of $\sigma_L = -50$ MPa, a negative lengthwise strain $\varepsilon_{tp,l} = -0.39$ % was determined, cf. Fig. 7a. Besides, the simulations are in good agreement with the experimental courses of the $\varepsilon_{tp,l}$. Corresponding to the volume constancy, diameter reductions were found for the transformation plasticity crosswise strains under tensile loading, while diameter increases were found under compressive loading, cf. Fig. 7b. As with the lengthwise strains, the final crosswise strains could also be modelled well, using the presented numerical model. However, especially regarding the crosswise strains under superimposed load, an altered transformation cinematic was found. As already observed by *Ahrens* [21], both tensile and compressive loads lead to an accelerated phase transformation. This effect results in different time courses between experiment and simulation as shown by the arrows in Fig. 7b. While in the experiment the strain increases significantly faster, in the simulation the strain increments take place with the same speed as in the stress-free state. However, in case of lengthwise strain, this effect is only slightly noticeable. This effect can be confirmed by visualising the evolution of the pearlitic phase fraction in Fig. 7c calculated via equation (7). It is clearly visible that especially the compressive stresses contribute to the accelerated phase transformation compared to the stress-free state. In order to deal with this effect numerically, it would be necessary to consider the effect of an accelerated phase transformation under superimposed loads in the ttt diagram. For this purpose, data such as transformation start and end times or martensite start and martensite finish temperatures would have to be considered in dependence on the stress.

All in all, the material data $(\Delta V_{tr}/V_0)_{A\rightarrow ph}$ and K_{ph}^{tp} could be calibrated successfully, so that the presented model was able to reproduce the experiments well. Calibrating the data to the numerical models in this way allows the material data to be implemented and used directly in other, more complex simulation models of hot forging in a next step.

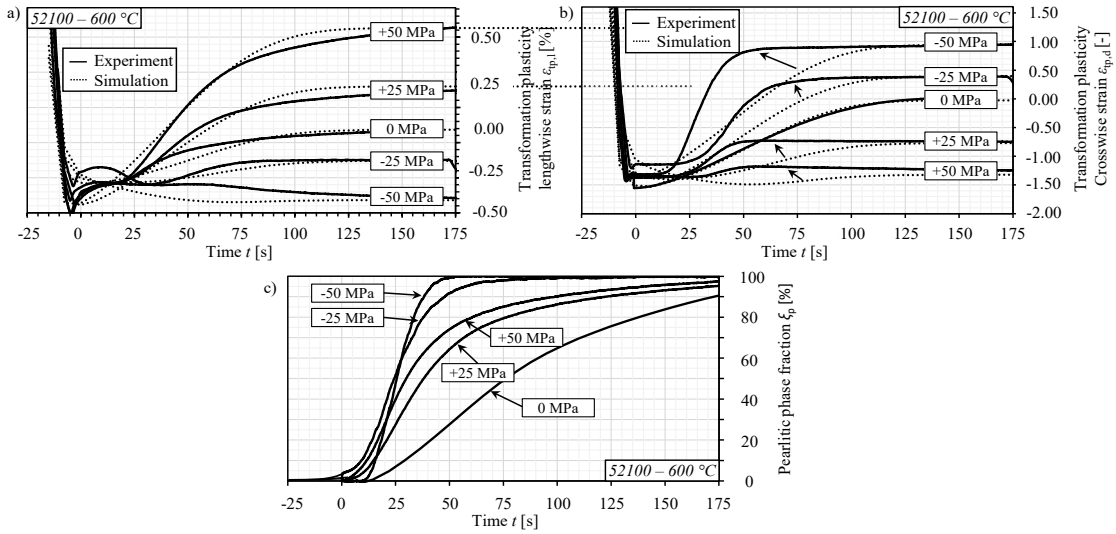

Fig. 7: Exemplary illustration of the results on the transformation plasticity of AISI 52100 during pearlitic phase transformation at 600 °C from experiments and simulations with regard to transformation plasticity lengthwise strain $\varepsilon_{tp,l}$ (a), transformation plasticity crosswise strain $\varepsilon_{tp,d}$ (b), as well as the evolution of the pearlitic phase fraction ξ_p during transformation(c).

Further results of the investigations on the transformation plasticity are summarised in Fig. 8 and in Table 3. It was found that both materials AISI 52100 as well as 4140 and each phase type has its own transformation plastic characteristics. In addition, the temperature influences the transformation plasticity behaviour. In particular, the ferritic/pearlitic phase transformation has a stronger transformation plasticity effect in contrast to the bainitic or martensitic transformation of the two materials. Overall, an increase of the transformation plasticity effects with rising temperature can be observed. Furthermore, under compressive stresses different K_{ph}^{tp} were observed than under tensile stresses, which is why a distinction is made in Table 3 between tensile and compressive stresses. The transformation plasticity tends to be more pronounced under tensile stresses than under compressive stresses, which was already noted in [13, 35].

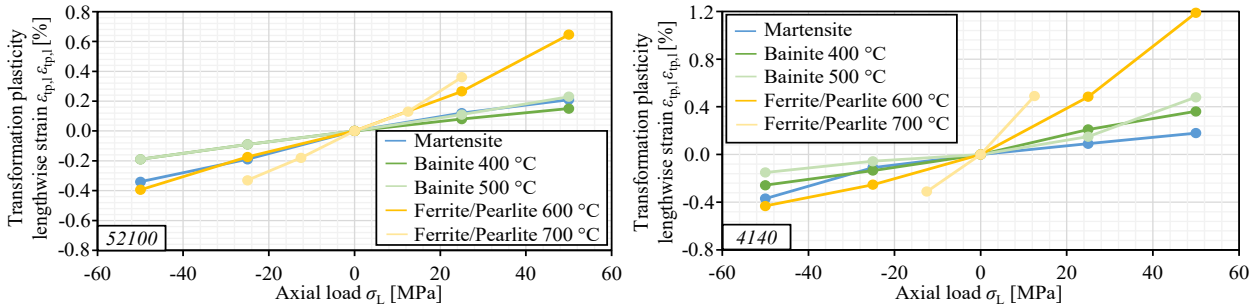

Fig. 8: Summary of the transformation plasticity lengthwise strains depending on the superimposed axial loads for different temperatures, phase types of materials AISI 52100 (a) as well as AISI 4140 (b).

Table 3: Summary of the coefficients of the transformation plasticity K_{ph}^{tp} with respect to material, phase type, temperature and stress type.

Phase type	**Cooling rate/ Temperature**	***Transformation plasticity coefficient K_{ph}^{tp} [10^{-5}*MPa^{-1}]***			
		AISI 52100		*AISI 4140*	
		Positive stress	*Negative stress*	*Positive stress*	*Negative stress*
Martensite	10 K/s	4.32	6.96	3.61	6.78
Bainite	400 °C	3.04	3.76	3.04	3.76
	500 °C	4.56	3.60	4.56	3.60
Pearlite	600 °C	12.46	7.70	12.46	7.70
	700 °C	13.44	13.60	13.44	13.60

Conclusion

In this paper, a methodology for researching the transformation plasticity effect was presented. The experimental tests were carried out on a Gleeble 3800-GTC using two extensometers to measure lengthwise and crosswise strains. In addition, the tests were numerically modelled using Simufact. Forming 16 to verify the data obtained and to further calibrate the data.

For a comprehensive investigation of the transformation plasticity strains and to simulate the transformation plasticity effect numerically, ttt data and characteristic data of the volumetric strains were determined in stress-free experiments and further calibrated in simulations. Subsequently, a database of experimentally determined and numerically calibrated transformation plasticity parameters was established. These data were provided for the materials AISI 52100 and 4140 phase- and temperature-specific as well as for compressive and tensile stresses.

The material data determined using the described method are directly suitable to use in further, even more complex simulation models. In a next step, the material data will be used to predict the distortions and residual stresses in a forging process of a complex demonstrator component inspired by a connecting rod. The overall aim is to enable the realistic virtual analysis of the important parameters of forging technology like distortions or residual stresses already in the course of process design by taking into account all occurring material effects and their interactions. This is intended to improve the process design in favour of the component properties.

Acknowledgement

This study was funded by the German Research Foundation (DFG, Deutsche Forschungsgemeinschaft) - 212963651 (BE 1691/142-2) as well as 374871564 (BE 1691/223-2) within the priority program SPP 2013.

References

[1] S. L. Semiatin, “Introduction to Forming and Forging Processes,” in *ASM Metals Handbook Volume 14 - Forming and Forging*, Totten, G., Howes, M., Inoue, T., Ed., Novelty, Ohio, USA, 1998.

[2] B.-A. Behrens *et al.,* “Numerical process design for targeted residual stress adjustment in hot bulk formed components taking into account macro- and microscale,” *Forsch Ingenieurwes*, vol. 85, no. 3, pp. 757–771, 2021, doi: 10.1007/s10010-021-00482-x.

[3] B.-A. Behrens *et al.,* “Experimental and Numerical Investigations of the Development of Residual Stresses in Thermo-Mechanically Processed Cr-Alloyed Steel 1.3505,” *Metals*, vol. 9, no. 4, p. 480, 2019, doi: 10.3390/met9040480.

[4] S. Denis, “Considering Stress-Phase Transformation Interactions in the Calculation of Heat Treatment Residual Stresses,” in *Mechanics of Solids with Phase Changes*, M. Berveiller and F. D. Fischer, Eds., Vienna: Springer Vienna, 1997, pp. 293–317.

[5] B.-A. Behrens and P. Olle, “Consideration of Phase Transformations in Numerical Simulation of Press Hardening,” *steel research international*, vol. 78, 10-11, pp. 784–790, 2007, doi: 10.1002/srin.200706286.

[6] B.-A. Behrens, A. Bouguecha, C. Bonk, and A. Chugreev, “Numerical and experimental investigations of the anisotropic transformation strains during martensitic transformation in a low alloy Cr-Mo steel 42CrMo4,” *Procedia Engineering*, vol. 207, pp. 1815–1820, 2017, doi: 10.1016/j.proeng.2017.10.944.

[7] E. Doege, H. Meyer-Nolkemper, and I. Saeed, *Fließkurvenatlas metallischer Werkstoffe: Mit Fließkurven für 73 Werkstoffe und einer grundlegenden Einführung*. München, Wien: Hanser, 1986.

[8] *Test Method for Youngs Modulus, Tangent Modulus, and Chord Modulus,* E28 Committee, West Conshohocken, PA.

[9] H. A. Kuhn, *Uniaxial Compression Testing*, 2000.

[10] *Test Method for Linear Thermal Expansion of Solid Materials With a Push-Rod Dilatometer,* E37 Committee, West Conshohocken, PA.

[11] *Practice for Quantitative Measurement and Reporting of Hypoeutectoid Carbon and Low-Alloy Steel Phase Transformations,* A01 Committee, West Conshohocken, PA.

[12] B.-A. Behrens, K. Brunotte, H. Wester, and C. Kock, "Targeted adjustment of residual stresses in hot-formed components by means of process design based on finite element simulation," *Arch Appl Mech*, vol. 91, no. 8, pp. 3579–3602, 2021, doi: 10.1007/s00419-021-01928-y.

[13] C. Şimşir, "3D finite element simulation of steel quenching in order to determine the microstructure and residual stresses," 2008.

[14] B.-A. Behrens and J. Schrödter, "Numerical Simulation of Phase Transformation during the Hot Stamping Process," *Thermal Process Modeling: Proceedings from the 5th International Conference on Thermal Process Modeling and Computer Simulation*, 2014.

[15] P. Olle, *Numerische und experimentelle Untersuchungen zum Presshärten*. Zugl.: Hannover, Univ., Diss., 2010. Garbsen: PZH Produktionstechn. Zentrum, 2010.

[16] H. P. Hougardy and K. Yamazaki, "An improved calculation of the transformation of steels," *Steel Research*, vol. 57, no. 9, pp. 466–471, 1986, doi: 10.1002/srin.198600805.

[17] A. Chugreev, "Numerische und experimentelle Untersuchungen zur Simulation von Rotationsreibschweißprozessen," Dissertation, TEWISS - Technik und Wissen GmbH, 2021.

[18] Sente Software Ldt., *JMatPro. Practical software for materials propertie.* [Online]. Available: https://www.sentesoftware.co.uk/jmatpro (accessed: Nov. 15 2021).

[19] Z. Guo, N. Saunders, P. Miodownik, and J. P. Schille, "Modelling phase transformations and material properties critical to the prediction of distortion during the heat treatment of steels," *IJMMP*, vol. 4, no. 2, p. 187, 2009, doi: 10.1504/IJMMP.2009.028632.

[20] M. Dalgic and G. Löwisch, "Einfluss einer aufgeprägten Spannung auf die isotherme, perlitische und bainitische Umwandlung des Wälzlagerstahls 100Cr6," *HTM Journal of Heat Treatment and Materials*, vol. 59, no. 1, pp. 28–34, 2004, doi: 10.3139/105.100271.

[21] U. Ahrens, *Beanspruchungsabhängiges Umwandlungsverhalten und Umwandlungsplastizität niedrig legierter Stähle mit unterschiedlich hohen Kohlenstoffgehalten*, 2003.

[22] J.-C. Videau, G. Cailletaud, and A. Pineau, "Experimental Study of the Transformation-Induced Plasticity in a Cr-Ni-Mo-Al-Ti Steel," *J. Phys. IV France*, vol. 06, C1, C1-465-C1-474, 1996, doi: 10.1051/jp4:1996145.

[23] F. Abrassart, "Stress-induced γ→ α martensitic transformation in two carbon stainless steels. Application to trip steels," *MT*, vol. 4, no. 9, pp. 2205–2216, 1973, doi: 10.1007/BF02643289.

[24] S. Sjöström, "Interactions and constitutive models for calculating quench stresses in steel," *Materials Science and Technology*, vol. 1, no. 10, pp. 823–829, 1985, doi: 10.1179/mst.1985.1.10.823.

[25] F. D. Fischer, E. R. Oberaigner, K. Tanaka, and F. Nishimura, "Transformation induced plasticity revised an updated formulation," *International Journal of Solids and Structures*, vol. 35, no. 18, pp. 2209–2227, 1998, doi: 10.1016/S0020-7683(97)00134-0.

[26] J. B. Leblond, J. Devaux, and J. C. Devaux, “Mathematical modelling of transformation plasticity in steels I: Case of ideal-plastic phases,” *International Journal of Plasticity*, vol. 5, no. 6, pp. 551–572, 1989, doi: 10.1016/0749-6419(89)90001-6.

[27] J. B. Leblond, “Mathematical modelling of transformation plasticity in steels II: Coupling with strain hardening phenomena,” *International Journal of Plasticity*, vol. 5, no. 6, pp. 573–591, 1989, doi: 10.1016/0749-6419(89)90002-8.

[28] A. Turetta, S. Bruschi, and A. Ghiotti, “Investigation of 22MnB5 formability in hot stamping operations,” *Journal of Materials Processing Technology*, vol. 177, 1-3, pp. 396–400, 2006, doi: 10.1016/j.jmatprotec.2006.04.041.

[29] G. Besserdich, B. Scholtes, H. Müller, and E. Macherauch, “Consequences of transformation plasticity on the development of residual stresses and distortions during martensitic hardening of SAE 4140 steel cylinders,” *Steel Research*, vol. 65, no. 1, pp. 41–46, 1994, doi: 10.1002/srin.199400924.

[30] B.-A. Behrens, A. Bouguecha, C. Bonk, and A. Chugreev, “Experimental investigations on the transformation-induced plasticity in a high tensile steel under varying thermo-mechanical loading,” *Computer Methods in Material Science*, no. 17, pp. 36–43, 2017.

[31] *DIN EN ISO 683-17:2015-02, Für eine Wärmebehandlung bestimmte Stähle, legierte Stähle und Automatenstähle_- Teil_17: Wälzlagerstähle (ISO_683-17:2014); Deutsche Fassung EN_ISO_683-17:2014*, Berlin.

[32] *DIN EN ISO 683-1:2018-09, Für eine Wärmebehandlung bestimmte Stähle, legierte Stähle und Automatenstähle_- Teil_1: Unlegierte Vergütungsstähle (ISO_683-1:2016); Deutsche Fassung EN_ISO_683-1:2018*, Berlin.

[33] B.-A. Behrens, A. Chugreev, and C. Kock, “Experimental-numerical approach to efficient TTT-generation for simulation of phase transformations in thermomechanical forming processes,” *IOP Conf. Ser.: Mater. Sci. Eng.*, vol. 461, p. 12040, 2018, doi: 10.1088/1757-899X/461/1/012040.

[34] *Aufstellung von Zeit-Temperatur-Umwandlungsschaubildern für Eisenlegierungen*, SEP 1680, Verein Deutscher Eisenhüttenleute, 2019.

[35] B.-A. Behrens, A. Chugreev, C. Kock, “Macroscopic FE-simulaion of residual stresses in thermo-mechanically processed steels considering phase transformation effects: XV International Conference on Computational Plasticity - Fundamentals and Applications: Barcelona, Spain, September 3-5, 2019,” Sep. 2019.